Bull. Mater. Sci. (2018) 41:135
https://doi.org/10.1007/s12034-018-1651-x

Confinement of an antiferroelectric liquid crystal in a polymer nanonetwork: thermal and dielectric behaviour

MARLIN BARAL*, A P RANJITHA and S KRISHNA PRASAD
Centre for Nano and Soft Matter Sciences, Bengaluru 560013, India
*Author for correspondence (marlin.baral@cens.res.in)

MS received 29 May 2018; accepted 23 September 2018; published online 10 October 2018

Abstract. We report the thermal and dielectric investigations on a liquid crystal exhibiting an antiferroelectric phase and confined in a polymer network of sub-micron dimensions. Two different photo-polymerizable monomers have been employed for the purpose: one of them (HDDA) is bereft of any aromatic parts, while the other (RM82) contains aromatic as well as aliphatic units and, in fact, forms a liquid crystalline phase in its monomeric state. The polymerization, which is carried out in the presence of the liquid crystalline host, is expected to yield a nanosegregated structure for HDDA and blended structure for the RM82 case, the difference reflecting the morphologies of the networks, as evidenced by SEM images. Surprisingly, even a small concentration of the latter polymer added to the former variety has substantial influence on the morphology. The main work focusses on calorimetry and dielectric relaxation spectroscopy of the host liquid crystal confined in these nanonetworks created by the polymers, which can be considered to form virtual surfaces with a finite anchoring energy. We have investigated the in-phase and antiphase modes in the antiferroelectric phase, and the soft mode in the paraelectric phase preceding the antiferroelectric phase. The relaxation frequencies of all these modes are substantially influenced by the network, with the results showing certain surprises in cases containing both HDDA and RM82.

Keywords. Nanonetwork; polymer confinement; antiferroelectric liquid crystal; dielectric relaxation spectroscopy.

1. Introduction

The nematic liquid crystal (LC) is an orientationally ordered fluid without any positional order. The phase is characterized by director (**n**) representing the average orientational direction of the constituent molecules. Introducing one-dimensional periodicity into the system, one realizes layered smectic phases: smectic A (SmA), if the director is along the layer normal, and smectic C (SmC), if it is at an angle. If the molecules are chiral, a precession of the **c** director between successive layers occurs, resulting in a macroscopic helix. A more important consequence of the chirality is the lowering of the symmetry of the structure, leading to the appearance of ferroelectricity in the chiral SmC (SmC*) phase [1]. In a variant of this phase, known as the antiferroelectric SmC* or SmC$^*_A$ phase, the **c** director points in almost opposite directions in the neighbouring layers [2]. This causes the polarization direction to alternate between the layers. A schematic representation of the molecular arrangement in these phases is depicted in figure 1a. Many interesting properties of the SmC$^*_A$ phase such as the tristate switching and double hysteresis loop in the polarization–electric ($P-E$) field have been well studied [3].

Confining LCs in a polymer network (PN) wherein the transverse dimension of the polymer structure is in the nanometre scale has attracted significant attention in recent times, not only due to the restricted geometry imparted by the network matrix on the liquid crystalline properties but also owing to their potential applications such as electro-optic devices [4–6]. The technological attraction of confining LC in a PN is that the latter protects the LC director configuration from distortions and mechanical shock. In these systems, such stabilization through the PN is realized by *in situ* photo-crosslinking of a small concentration of photoreactive monomers. The network provides virtual surfaces inside the LC cell, thereby significantly influencing the behaviour of the LC substance. A number of studies reporting such influences with LCs confined in PNs exist in the literature, but focussed on the nematic or the ferroelectric SmC* phase [7–9]. For example, Kossyrev *et al* [10] found that the confinement in polymer bundles improved the switch-off dynamics of the device of rod-like molecules. In the case of ferroelectric LCs, the network resulted in decrease (increase) of the dielectric strength (relaxation frequency) associated with a process referred to as the Goldstone mode (GM). In contrast, the soft mode (SM) parameters were essentially unaltered [11]. As opposed to the focus on the nematic and ferroelectric LCs, studies on the polymer-stabilized antiferroelectric (PSAFLC) structure are only a few [12–15], with only one on the dielectric properties [15]. The nature of the polymer has an important say in the behaviour [16]. If it is non-aromatic (referred to as Type A here), nanophase segregation is favoured with the polymer chains getting imbibed between the layers of LC molecules. On the contrary, a polymer formed

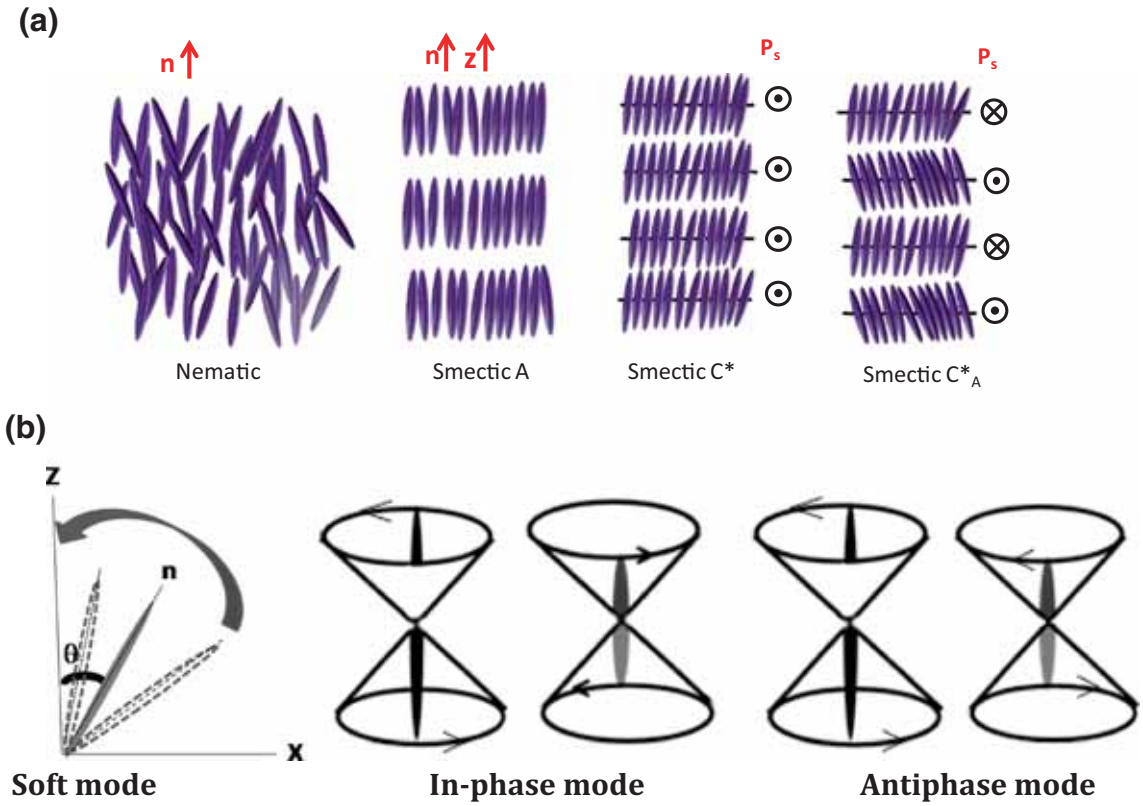

Figure 1. (**a**) Schematic diagram of the molecular arrangement in the different liquid crystal phases discussed. Of specific interest are the layered smectic A phase, which exhibits paraelectric behaviour, and the smectic CA* phase with its antiferroelectric character arising from the molecular tilt alternation from layer to layer; **n** and **Z** indicate the directions of the director and the layer normal, respectively. $\mathbf{P_s}$ indicates the direction of the polarization, which alternates between neighbouring layers. (**b**) Schematic diagram for various collective dielectric relaxation processes described in the article.

by mesogenic monomers (Type B) would have a strong tendency to follow the ordering of the LC molecules. These differences do alter the physical properties substantially, as was demonstrated by Madhuri *et al* [15] and Labeeb *et al* [17]. In this article we demonstrate the effect of the polymer confinement on the dielectric properties of an LC exhibiting a direct transition from the paraelectric SmA to the antiferroelectric SmC^*_A phase. Comparison is performed between the situations wherein the polymer is Type A or Type B.

Keeping the broad readership in mind, we provide a brief description of the dielectric processes involved [18–21]. The SmC^* shows the GM and SM, both of which are collective in nature: while GM corresponds to the fluctuation of the azimuthal angle (phase) ϕ around the helical axis, SM originates from the fluctuation of the polar (amplitude) angle θ of the two-component tilt order parameter. In the SmA phase, these two modes become degenerate and only SM prevails. On the other hand, in the SmC^*_A phase, two possible types of azimuthal angle fluctuations give rise to two modes: the antiphase mode (AM) and the in-phase mode (IM). Apart from these modes, the phases also show two molecular processes due to molecular rotation about the long and short molecular axes. A schematic representation of these modes is provided in figure 1b. The AM has invoked much interest even from a technological point of view, owing to the potential to realize a photonic switch with nanosecond response times; see e.g. [22].

2. Experimental

The host LC 4-(1-(trifluoromethylheptyloxy carbonyl) phenyl 4′-octyloxybiphenyl 4-carboxylate (TFM for short) was procured from Aldrich, and used as received. The photopolymerizable monomers employed are HDDA (from Aldrich) and RM82 (from E-Merck), and belong to Type A and Type B categories mentioned earlier. The chemical structures and transition temperatures (where applicable) of these compounds are presented in table 1. Experiments have been conducted on pure TFM, and materials comprising the polymers. The latter are labelled as TFM10HD, TFM9HD1RM and TFM10RM, where HD and RM stand for HDDA and RM82, respectively, and the numerals their concentration (in weight%) in the composite; TFM9HD1RM consists of 9 wt% HD and 1 wt% of RM82. The mixture with RM82 was prepared by physically mixing the components while maintaining the sample in the isotropic phase.

Table 1. Molecular formulae along with the phase sequences of the host LC TFMHPOBC, the photoactive monomers HDDA and RM82 and the catalyst BME.

Compound	Molecular formula	Phase sequence
TFMHPOBC	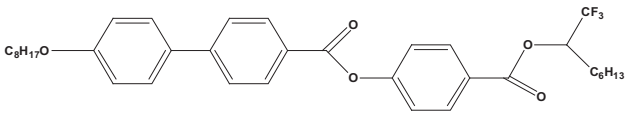	Iso 125.1°C SmA 116°C SmC_A 68°C Cr
HDDA	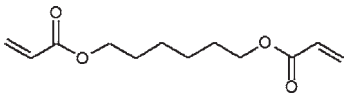	
RM82	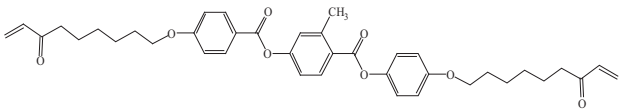	Iso 118°C N
BME	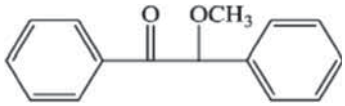	

The mixture with HDDA was prepared by solvent mixing using toluene. The solution was then sonicated for 10 min followed by solvent evaporation at 110°C. To ensure complete evaporation of the solvent, the sample was kept in vacuum for 6 h. The polymerization of monomers was performed by including a small quantity (2%) of a photoinitiator (BME, Aldrich), and illuminating the sample contained in a sandwich cell (to be described later) with a low-power (2 MW cm^{-2}) UV lamp with a peak wavelength of 365 nm. The cells employed were fabricated with indium–tin oxide (ITO)-coated glass plates, pre-treated with a polymer alignment layer to achieve homogeneous planar alignment of the molecules. Dielectric relaxation spectroscopy (DRS) measurements were carried out over a frequency range of 10^2–10^7 Hz using an impedance analyser (HP4194A). A schematic diagram of its experimental set-up is shown in figure 2. FESEM images of the polymer morphologies were obtained using a MIRA 3 LHU (model Tescan). Differential scanning calorimetry (DSC) studies were carried out using a power-compensated DSC (Model 8000, Perkin-Elmer). To perform the SEM analysis, the sandwich cell containing the polymerized sample was immersed in acetone for 48 h to leech out the confined LC. Then, the cell was opened up and allowed to stay at room temperature to drive out any solvent that may be left over, following which the microscopy study was performed.

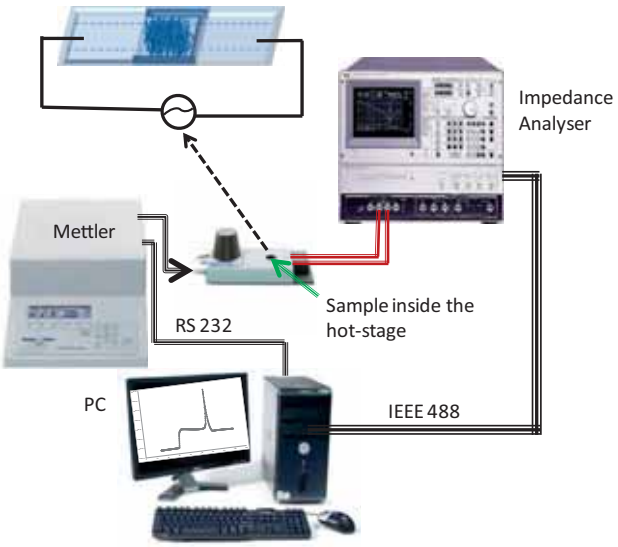

Figure 2. Experimental set-up used for the dielectric experiments.

3. Results and discussion

3.1 *Morphology of the PN*

The SEM images presented in figure 3a–c clearly indicate that the morphologies are significantly different in the three cases. The HDDA-only system (figure 3a) shows short strands, which run parallel to each other only on a local scale, with a number of them looping around. The RM82-only film presents longer strands (figure 3b). A surprising feature occurs in the two-polymer system, TFM9HD1RM: the morphology is more of an interconnected one, almost mimicking a droplet structure (figure 3c). However, on local scales, the parallelism of the strands is far better defined in this case, than in the other two (inset of figure 3c). The mutual influence of the two polymers in altering the morphology requires a detailed study.

3.2 *Calorimetry*

Figure 4 presents the calorimetric scans obtained in the cooling mode at a rate of 5°C min^{-1}. In all the cases, signatures of the isotropic–SmA and SmA–SmC_A^* transitions

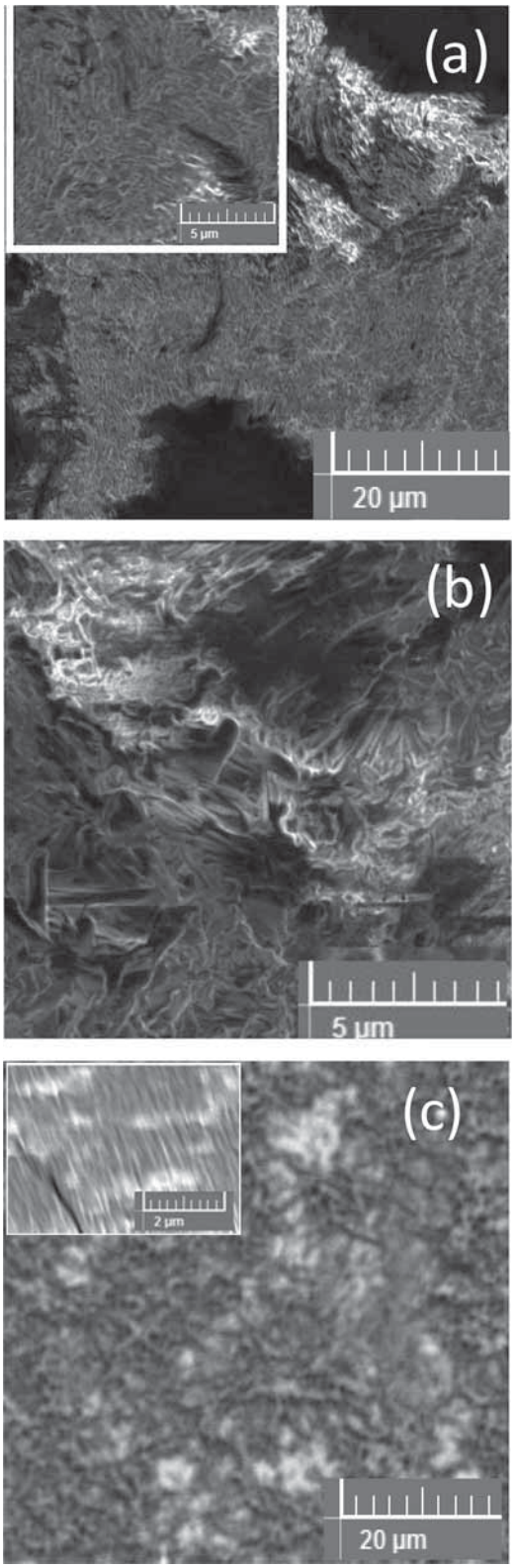

Figure 3. FESEM images of the polymer networks after taking out the confined liquid crystal for the (**a**) TFM10HD, (**b**) TFM10RM and (**c**) TFM9HD1RM samples, exhibiting significant morphological differences. The fibrillar structures have lateral dimensions in the nanometre scale.

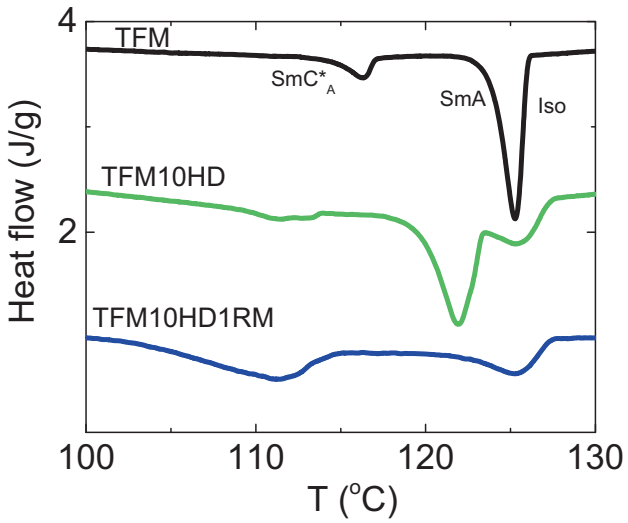

Figure 4. Differential scanning calorimetric scans for the three samples exhibiting the isotropic–smectic A and smectic A–smectic C^*_A transitions. The TFM10HD samples exhibit two thermal signatures in the vicinity of the former transition, and the higher temperature is attributed to the surface effect.

are clearly seen, in spite of notable exceptions in the polymer-networked samples. Firstly, the profiles become broader, especially in the case of the transition between the smectic phases. Secondly, while the 2-polymer case has a single thermal anomaly corresponding to the Iso–SmA transition, the HDDA-only sample has two peaks; this difference is observed for the smectic–smectic transition also, although it is far less prominent. The peak temperature of the higher temperature one coincides with that for the pure TFM sample. Observing doublet peaks for the clearing point transition is not uncommon in confined samples, and often associated with two events [23–26], one occurring at the surface and the other in the interior. The nanoconfinement situations accentuate this owing to the proliferation of the virtual surfaces created by the confining entity, which in the present case are the polymer fibres. As already mentioned in the introduction, the presence of HDDA gives rise to a nanosegregation scenario whereas the RM82 polymer is along the director direction, at least in the SmA phase. Thus, the (polymer) surface effects are much stronger in the HDDA case, than in the RM82 case. More surprisingly, in the TFM9HD1RM case, the presence of even 1% RM82 diminishes the effect due to HDDA, although the latter is in a larger quantity. Studies related to the concentration should bring out the relative influence of the two polymers.

3.3 *Dielectric behaviour: fixed frequency data*

The thermal variation of the permittivity, $\varepsilon_\perp$, for the different materials is presented in figure 5. The signature of the Iso–SmA transition is hardly seen, and the behaviour is dominated by the peak-like feature marking the SmA−SmC^*_A

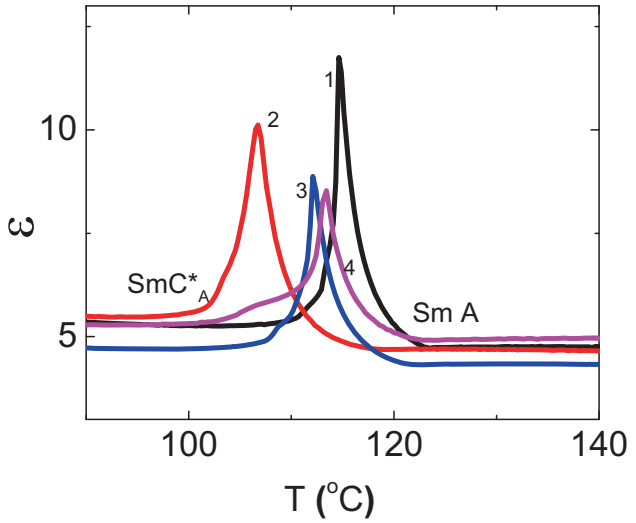

Figure 5. Thermal variation of ε, the permittivity perpendicular to the **n** director across the smectic A–smectic C^*_A transition for (1) pure TFM, (2) TFM10HD, (3) TFM9HD1RM and (4) TFM10RM samples. In all cases, the transition is signified by a peaking of the data, although the magnitudes are different, with pure TFM having the highest strength, and TFM10RM, the lowest.

transition. The presence of the peak signifies that the SM contribution dominates the overall variation. The qualitative feature essentially remains the same for the pure LC and the polymer-networked systems. However, the peak value diminishes in the networked cases, with the RM82-only network having the smallest magnitude. Again, the mixed polymer material shows that in the two-polymer case, even though RM82 is the minority component (1%), the behaviour is dominated by it. It is important to note that peak temperatures for the different cases corroborate the transition temperatures as obtained by DSC.

3.4 *DRS*

The raw DRS profiles of the frequency (f) dependence of imaginary (ε'') parts of the permittivity in the SmC^*_A phase for pure TFM and a representative PN sample, viz., TFM10HD, are shown in figure 6a and b, respectively. Evidently, two relaxation processes are present in both the samples. Our earlier analysis [15] has clearly established that the low-frequency mode, lying in the range of tens of kHz, is the IM mode, while the higher frequency one, in the MHz region, is the AM. The profiles in the SmA phase exhibit a single relaxation arising from the SM relaxation, as seen in figure 6a. To obtain the relaxation parameters, the raw profiles of ε'' *vs.* f were fit to the Havriliak–Negami (HN) equation [27]:

$$\varepsilon^*(f) = \varepsilon_\infty + \frac{\Delta\varepsilon}{[1 + (if/f_R)^\alpha]^\beta} + i\frac{\sigma_o}{f^N} + iAf^m \qquad (1)$$

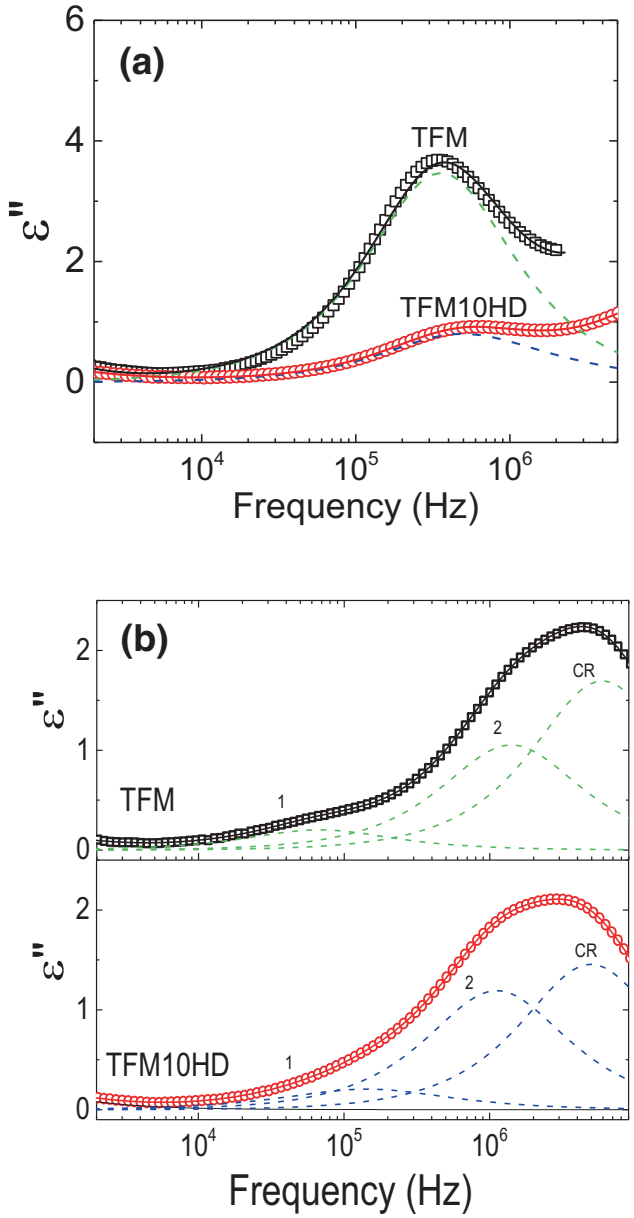

Figure 6. Raw dielectric absorption (ε'') profiles in the (**a**) SmA and (**b**) SmC^*_A phases of TFM and TFM10HD samples. Apart from the process due to the cell relaxation (labelled as CR), the SmA phase (T = 116°C) shows only one mode, associated with the soft mode fluctuations, whereas the SmC^*_A (T = 98°C) exhibits two modes corresponding to the (1) in-phase and (2) antiphase processes. The solid line represents the fit to the HN expression (equation 1), whereas the dashed lines represent contributions of the individual modes.

Here $\varepsilon^*(f)$ is the complex permittivity at the measuring frequency f and ε_∞ is the high-frequency permittivity, which includes contributions from any high-frequency modes that may exist, other than the ones considered. The second term is the HN contribution, where f_R is the relaxation frequency and $\Delta\varepsilon$ the corresponding dielectric strength; α and β are the profile-shape parameters; the situation $\alpha, \beta = 1$ represents

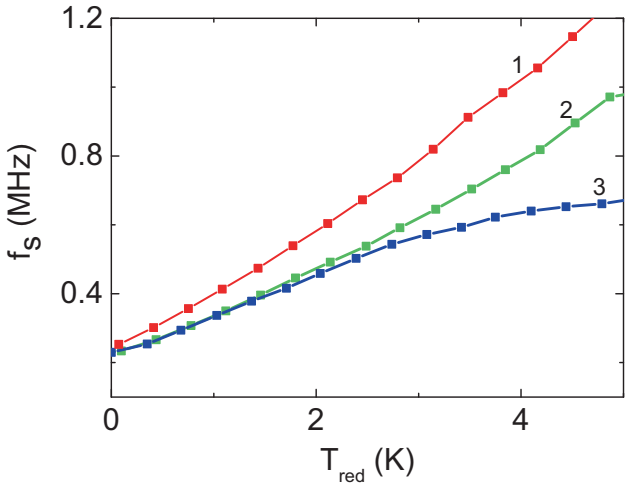

Figure 7. Temperature dependence ($T_{red} = T - T_c$) of the soft mode relaxation frequency for (1) TFM, (2) TFM10HD and (3) TFM9HD1RM samples.

Debye relaxation. The profiles in the SmA phase required only one HN term, while those in the SmC_A^* phase required two. The third term in equation (1) accounts for contributions from the DC conductivity (σ_o), while the last term is included to take care of the contributions from the finite sheet resistance of the substrate electrodes. The complete fits as well as the de-convoluted individual contributions are also shown in figure 6a and b. For all the modes investigated, the parameters α and β took value 1, indicating that the process is Debye-like.

Figure 7a shows the temperature dependence of f_s, the relaxation frequency of the SM for TFM and the two PN samples, TFM10HD and TFM9HD1RM. The overall behaviour in all the cases is as expected: f_s increases as $T - T_c$ increases, i.e., on moving away from the SmA–SmC_A^* transition (here T_c is the SmA–SmC_A^* transition temperature). However, while the former two exhibit a continuously increasing frequency, TFM9HD1RM has a limiting behaviour at high $T - T_c$. The interesting feature is that the presence of the PN lowers the relaxation frequency, suggesting that the hindrance to the associated tilt fluctuations is reduced when the sample is confined in the PN. The thermal behaviour observed can be described by the following expression obtained from a Landau analysis constructed for the SmA–SmC^* transition (in the absence of an analysis specific to antiferroelectric systems, we employ the expressions proposed for materials exhibiting paraelectric–ferroelectric transition, see e.g. [28]):

$$f_s = \frac{\alpha(T - T_c) + \left(K - \varepsilon\mu^2\right) q^2}{2\pi\eta_s} \qquad (2)$$

Here α, μ, K, q and η_s are, respectively, the Landau coefficient connected with the quadratic term of the order parameter in the tilted phase, the flexoelectric coefficient,

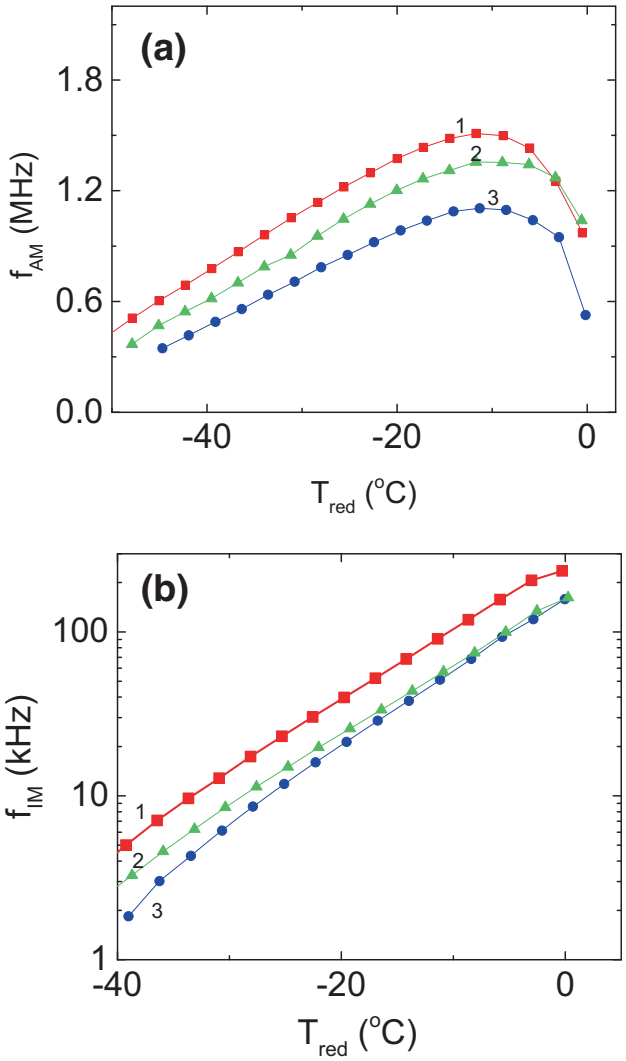

Figure 8. Temperature dependence of the (**a**) antiphase and (**b**) in-phase modes relaxation frequency for (1) TFM, (2) TFM10HD and (3) TFM9HD1RM samples.

the Frank elastic coefficient, the wave vector of the helix and the viscosity associated with the SM. Owing to the limiting behaviour in TFM9HD1RM, we have considered data in the range $T - T_c = 0$–3 K for the fit to equation (2), whose slope yields the ratio α/η_s. The best fit to the data gives this ratio to be $(17.97 \pm 0.3) \times 10^{-4}$, $(13.25 \pm 0.2) \times 10^{-4}$ and $(11.77 \pm 0.2) \times 10^{-4} K^{-1} s^{-1}$ for TFM, TFM10HD and TFM19HD1RM, respectively. This indicates that although the two-polymer material gives a lower magnitude of f_s far away from the transition to the SmC_A^* phase, its temperature dependence in the vicinity of the transition is quite similar to that of the HDDA-only composite. With the determination of the α value, one should be able to extract the SM viscosity in each of these cases, and also find out the reason for f_s to show a limiting behaviour away from the transition in the case of TFM19HD1RM.

The temperature dependences of the antiphase relaxation frequency f_{AM} in the SmC^*_A phase for TFM and the networked samples are shown in figure 8. All the materials exhibit a similar behaviour with a rapid increase near T_c, and after reaching a maximum, a gentle decrease with further lowering of temperature. Interestingly, the maximum value is achieved at about $T_c - 10$ K. Confining in the network does decrease at any $T_c - T$ point. Further, the reduction is the highest for the single polymer containing TFM10HD, with the 2-polymer component TFM9HD1RM having values between the two sets. Taking the ratio of maximum f_{AM} values of the pure TFM to those of the networked samples, it is seen that the reduction is 10% for TFM9HD1RM and 34% for TFM10HD samples. Interestingly, the data on TFM10RM reported by Madhuri *et al* [15] also exhibit 34% reduction. Thus, it appears that although the polymer content is approximately the same, the single-polymer systems are more efficient in lowering f_{AM}, unlike in the case of the SM relaxation. This is not true for the relaxation frequency of the IM, f_{IM}. There is a diminution in the value when the sample is confined in the PN, but the difference between TFM9HD1RM and TFM10HD samples can be seen only deep in the SmC^*_A phase. Further, the data for TFM10RM are essentially identical to those for the pure TFM sample. Thus, it is clear that that the nature of the polymer has a strong influence on the dielectric modes in the SmC^*_A phase as well. Detailed tilt angle, polarization and bias-dependent dielectric measurements are required to get a full grasp of the behaviour in the PN confinement. These experiments, which are in progress, are expected to throw light on the influence due to finite length scale achieved by confinement as well as the wall forces of the polymer in governing the dielectric behaviour of these systems exhibiting paraelectric–antiferroelectric transformation.

4. Conclusions

We have carried out thermal and dielectric measurements on an LC confined in PNs. The host LC exhibits a direct transition from a paraelectric phase to an antiferroelectric phase. The morphologies of the PNs formed are evidently dependent on the chemical nature of the monomer; as the polymerization is carried out *in situ* (in the presence of the LC) it adopts either a nanosegregated structure or a blend with the host layers. These differences are seen to have strong influence on the DSC as well the results of DRS. Encouraged by these results, we are conducting measurements of related parameters like tilt angle, polarization and bias dependence of permittivity that are expected to provide a comprehensive picture of the issues governing the behaviour of the relaxation modes.

References

[1] Chandani A D L, Ouchi Y, Takezoe H, Fukuda A, Furukawa K and Kishi A 1989 *Jpn. J. Appl. Phys.* **28** L1261

[2] Musevic I, Blinc R and Zeks B 2000 *The physics of ferroelectric and antiferroelectric liquid crystals* (Singapore: World Scientific)

[3] Fukuda A, Takanishi Y, Isozaki T, Ishikawa K and Takezoe H 1994 *J. Mater. Chem.* **4** 997

[4] Crawford G P and Zumer S (eds) 1996 *Liquid crystals in complex geometries: formed by polymer and porous networks* (Boca Raton: CRC Press)

[5] Dierking I 2014 *Materials* **7** 3568

[6] Kumar R and Raina K K 2011 *AIP Conf. Proc.* **1393** 46

[7] Archer P, Dierking I and Osipov M A 2008 *Phys. Rev. E: Stat. Nonlin. Soft Matter Phys.* **78** 051703

[8] Tan G, Lee Y H, Gou F, Chen H, Huang Y, Lan Y F *et al* 2017 *J. Phys. D: Appl. Phys.* **50** 493001

[9] Blinc R, Musevic I, Pirs J, Skarabot M, Zeks B, Crawford G P *et al* 1996 *Liquid crystals in complex geometries: formed by polymer and porous networks* (Boca Raton: CRC Press)

[10] Kossyrev P A, Qi J, Priezjev N V, Pelcovits R A and Crawford G P 2002 *Appl. Phys. Lett.* **81** 2986

[11] Petit M, Hemine J, Daoudi A, Ismaili M, Buisine J M and Costa D A 2009 *Phys. Rev. E: Stat. Nonlin. Soft Matter Phys*. **79** 031705

[12] Strauss J and Kitzerow H S 1996 *Appl. Phys. Lett.* **69** 725

[13] Rudquist P, Elfström D, Lagerwall S T and Dabrowski R 2006 *Ferroelectrics* **344** 177

[14] Furue H and Yokoyama H 2003 *J. Appl. Phys.* **42** 6180

[15] Madhuri P L, Prasad S K and Nair G G 2014 *RSC Adv.* **4** 3121

[16] Guymon C A, Hoggan E N, Clark N A, Rieker T P, Walba D M and Bowman C N 1997 *Science* **275** 57

[17] Labeeb A, Gleeson H F and Hegmann T 2015 *Appl. Phys. Lett.* **107** 232903

[18] Kremer F and Schonhals A (eds) 2003 *Broadband dielectric spectroscopy* (Berlin: Springer)

[19] Mishra A, Dabrowski R and Dhar R 2018 *J. Mol. Liq.* **249** 106

[20] Parry-Jones L A and Elston S J 2001 *Phys. Rev. E: Stat. Nonlin. Soft Matter Phys*. **63** 050701

[21] Das D, Lahiri T and Majumder T P 2011 *Physica B: Condens. Matter* **406** 1577

[22] Song J, Manna U, Fukuda A and Vij J K 2008 *Appl. Phys. Lett.* **93** 142903

[23] Dadmun M D and Muthukumar M 1993 *J. Chem. Phys.* **98** 4850

[24] Caggioni M, Roshi A, Barjami S, Mantegazza F, Iannacchione G S and Bellini T 2004 *Phys. Rev. Lett.* **93** 127801

[25] Jayalakshmi V, Nair G G and Prasad S K 2007 *J. Phys.: Condens. Matter* **19** 226213

[26] Kumar V and Prasad S K 2012 *RSC Adv.* **2** 8531

[27] Havriliak S and Negami S 1966 *J. Polym. Sci. C* **14** 99

[28] Carlsson T, Žekš B, Filipič C and Levstik A 1990 *Phys. Rev. A* **42** 877